Editors' Suggestion | Featured in Physics

# Twenty-Five-Fold Reduction in Measurement Uncertainty for a Molecular Line Intensity

Adam J. Fleisher,* Erin M. Adkins, Zachary D. Reed, Hongming Yi, David A. Long, Hélène M. Fleurbaey, and Joseph T. Hodges†

*National Institute of Standards and Technology, 100 Bureau Drive, Gaithersburg, Maryland 20899, USA*

(Received 24 April 2019; revised manuscript received 6 June 2019; published 24 July 2019)

To accurately attribute sources and sinks of molecules like $CO_2$, remote sensing missions require line intensities ($S$) with relative uncertainties $u_r(S) < 0.1\%$. However, discrepancies in $S$ of $\approx 1\%$ are common when comparing different experiments, thus limiting their potential impact. Here we report a cavity ring-down spectroscopy multi-instrument comparison which revealed that the hardware used to digitize analog ring-down signals caused variability in spectral integrals which yield $S$. Our refined approach improved measurement accuracy 25-fold, resulting in $u_r(S) = 0.06\%$.

DOI: 10.1103/PhysRevLett.123.043001

The oscillator strengths of atoms and molecules are, to a high degree of precision, considered invariants of nature and therefore benchmark values for testing fundamental theories of physics and chemistry. The simplest many-body system in nature is the neutral helium atom, whose accurately known oscillator strengths enable validations of various electronic structure theory approximations [1]. Accurate oscillator strengths for molecular hydrogen (and other molecules) are used to model spectra from distant parts of the Universe, and thus constrain variations in the proton-electron mass ratio [2–4], while improved observational and modeling capabilities have leveraged known oscillator strengths to constrain the isotope composition of our Solar System [5] and the Universe [6]. More generally, accurate measurements of oscillator strengths for both resonant molecular transitions [7] as well as collision-induced absorption [8] provide important constraints on *ab initio* dipole moment surfaces which predict light-matter interactions for such seemingly intractable extreme environments as exoplanetary atmospheres (see, e.g., Ref. [9]).

Closer to home, remotely located spectrometers designed to answer fundamental questions concerning Earth's atmosphere also leverage accurately known oscillator strengths (and their derived quantities) to predict light-matter interactions and quantify trends in atmospheric composition. Often, however, independent validation of the dynamic and spatially variable atmospheric samples under study is extremely difficult, if not impossible. In those cases, improved accuracy in the spectroscopic models would reduce or eliminate the need for costly validation experiments.

For example, the high-resolution JAXA Greenhouse Gases Observing Satellite (GOSAT) [10] and NASA Orbiting Carbon Observatory (OCO) [11] passive remote sensing missions have, for more than a decade, relied upon accurate spectroscopic forward models of carbon dioxide ($CO_2$) and molecular oxygen ($O_2$) to retrieve $CO_2$ column densities: the measurement target being a precision of 1 $\mu$mol/mol, or approximately 0.3% of the nominal mean column density [12–14]. Additionally, monitoring global trends in atmospheric methane ($CH_4$) [15–18] and performing point-source attribution [19] currently motivates laboratory research into accurate first-principles models in congested spectral regions [20,21], and open-path dual-comb spectroscopy has achieved the following low relative instrumental variations for mole fractions at 30 s of integration: 0.14% for $CO_2$, 0.35% for $CH_4$, and 0.40% for water ($H_2O$) [22]. Consequently, reference values for the absorption cross sections (derived from the oscillator strengths) of these and many more molecules (see, e.g., Ref. [23]) must be known with sufficiently low relative uncertainty ($\leq 0.1\%$) to ensure accurate retrievals from highly precise instruments.

The spectroscopic model for light-matter interactions which relates an observable like spectral transmittance ($\mathcal{T}$) to the mole fraction of absorbing molecules ($\chi$) along a path length ($L$) is expressed as

$$\chi = -\frac{\ln(\mathcal{T}) k_B T}{\sigma p L}, \tag{1}$$

where $k_B$ is the Boltzmann constant, $T$ is the temperature, $p$ is the pressure, and $\sigma$ is the absorption cross section. Assuming that $\mathcal{T}$ is the experimental observable (along with $T$, $p$, and $L$), a suitable model for $\sigma$ will yield an accurate measurement of $\chi$. At values of $T$ and $p$ routinely encountered within Earth's atmosphere, $\sigma$ can comprise a relatively smooth function of frequency $\nu$ in congested spectral regions (e.g., volatile organic compounds in air [24,25]), or when the absorber lifetime is short (e.g., collision-induced absorption [8]). When clusters of overlapping lines are resolved (e.g., the overtone spectrum of methane [20,21]), we can express $\sigma$ as a summation over a physically justified choice of line shape profiles (including line mixing) scaled by the respective molecular line

intensities ($S$), which can be calculated in terms of invariants of nature. Importantly, this approach yields first-principles models for $\sigma$.

In the simplest line-by-line spectral model, $\sigma$ for small molecules like $CO_2$ can be expressed as a sum over $j$ well-isolated spectral lines using their known values of $S_j$ and the real parts of their respective line shape functions $g_j(\nu)$:

$$\sigma = c\sum_j S_j g_j(\nu) + \cdots. \tag{2}$$

In Eq. (2), $c$ is the speed of light and the ellipsis implies additional broadband terms (e.g., spectral baseline). Together, Eqs. (1) and (2) illustrate a well-known fact: uncertainties in the values of $S$ (and more generally $\sigma$) will propagate linearly into uncertainty in atmospheric retrievals of $\chi$ (see, e.g., Ref. [12]).

Currently, state-of-the-art *ab initio* calculations of $S$ report relative standard uncertainties $u_r(S)$ of about 1%, and preliminary comparisons with the most accurate available experimental data suggest an agreement of better than 1% for some rotationally resolved vibrational bands (see, e.g., Refs. [7,26–29]). However, comparisons between theory and a single optical instrument may be insufficient to capture all type-$B$ (systematic) uncertainty. Unfortunately, line intensities measured across experiments like Fourier-transform spectroscopy, cavity-enhanced absorption spectroscopy, and/or cavity ring-down spectroscopy (CRDS) are known to vary by 1%–2% [29]. Therefore, establishing by consensus the most accurate values and uncertainties for $S$ remains a work in progress [30].

Here we report a multi-instrument comparison between $S$ recorded using three unique CRDS instruments at the National Institute of Standards and Technology (NIST) in Gaithersburg, Maryland. The experiments were performed over a time period of greater than one year. Our goal was to evaluate the origin and magnitude of the dominant sources of systematic uncertainty in the measurement of $S$ of an individual $CO_2$ transition, an experimental observable that is proportional to an invariant of nature [29]. We find that, in addition to the standard controls and measures of sample temperature, pressure, optical frequency, line shape profile, and certified absorber mole fraction, a quantitative evaluation of previously uncharacterized CRDS signal digitizer nonidealities was required to reduce $u_r(S)$ to our minimum achieved value of $u_r(S) = 0.06\%$. By calibrating numerous CRDS digitizers using a metrology-grade reference digitizer with high static linearity and synthetic exponential decay signals (SEDS), we achieved a 25-fold reduction in $u_r(S)$ relative to the current literature value of $u_{\mathrm{lit}}(S) = 1\%$–$2\%$ [29]. Using this approach, we met the long-standing goal of quantifying $S$ with sufficient precision and accuracy needed in first-principles calculations of absorption cross sections for the most ambitious optical remote sensing missions. Moreover, we achieved this goal for the $CO_2$ transition under consideration for active remote sensing by the NASA Active Sensing of $CO_2$ Emissions over Nights, Days, and Seasons (ASCENDS) mission [31].

In an idealized CRDS experiment performed with a single-frequency continuous-wave laser, the passive decay of optical power from a high-finesse optical resonator is purely exponential, and the cavity time constant ($\tau$) encodes the round-trip intracavity losses (e.g., molecular absorption). Generally, optical decays are converted to analog electrical signals by a photoreceiver and then digitized by an analog-to-digital converter for software analysis. Deviations from purely exponential behavior arising from common sources like photoreceiver saturation, incomplete laser shuttering, or interfering optical resonator modes are readily identified by systematic residuals in the fitted decays. However, slight nonidealities in the digitizer hardware are not so readily identified and could be particularly problematic for nonlinear CRDS methods [32]. To date, only large digitizer nonidealities have been discussed in the CRDS literature [33]. Here we hypothesize that each of our common digitizers has a unique power law response that governs its static linearity, and that slight deviations from a unity exponent in that power law systematically alter the observed values of $\tau$ without introducing nonexponential time dependence of the digitized electronic signals.

A general illustration of the CRDS approach is shown in Fig. 1. While each of the three spectrometers used here were unique, they shared several common properties.

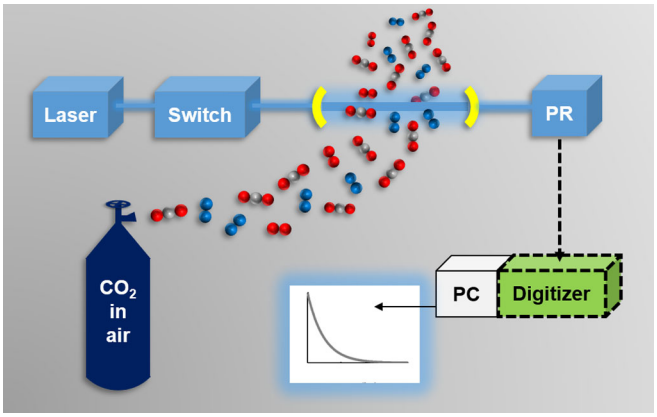


FIG. 1. General illustration of a cavity ring-down spectrometer. From the top left, a continuous-wave laser (blue lines) was injected into an optical cavity (yellow curved mirrors) containing a flowing gas sample of $CO_2$ in air (gray, carbon; red, oxygen; blue, nitrogen). Upon reaching a predefined transmission threshold, an optical switch shuttered the laser and passive cavity decays were observed incident on a photoreceiver (PR). The electrical output of the PR (black dashed arrow) was coupled to an analog-to-digital converter (or digitizer), and the resulting digitized decay signals were fitted in real time using homebuilt acquisition software and a personal computer (PC).

The central component of each instrument was a high-finesse, linear two-mirror optical resonator which contained a flowing gas sample (actual volumetric flow rates of 0.02–0.04 L/ min) of NIST standard reference material (SRM) gas mixture 1721-A-29, Southern Oceanic Air, with a certified $CO_2$ mole fraction of $\chi_{CO_2} = (387.98 \pm 0.05)$ $\mu$mol/mol $[u_r(\chi_{CO_2}) = 0.013\%]$ [34,35]. For each instrument, a continuous-wave laser was spatially mode matched and injected into the stable optical resonator to interrogate $CO_2$ absorption, specifically the $R$ 16$e$ $^{12}C^{16}O_2$ rotational transition within the 30012—00001 vibrational band (center wave number of $\tilde{\nu}_0 = 6359.967$ cm$^{-1}$ [29]). Following optical buildup to a predetermined transmission threshold, the probe laser was optically shuttered and passive cavity decays were observed on a photoreceiver, digitized, and fitted in real time with an exponential decay to provide the $\tau$ as a function of laser frequency.

All three CRDS instruments utilized here were previously reported in part. Spectrometer 1 ($S1$) was a frequency-stabilized (FS) CRDS [36] instrument with a nominal cavity length $L = 139$ cm, single-pass base losses $\ell = 3.3 \times 10^{-5}$, laser line width of $\delta \approx 100$ kHz, photoreceiver minimum noise-equivalent power of NEP $= 0.34$ pw Hz$^{-1/2}$ and electronic bandwidth of $B = 8$ MHz, and optical trigger threshold of $V_{trig} = 1$ V [37]. Spectrometer 2 ($S2$) was also an FS-CRDS instrument, but with nominal $L = 75$ cm, $\ell = 1.68 \times 10^{-4}$, $\delta \approx 300$ kHz, NEP $= 0.34$ pw Hz$^{-1/2}$ and $B = 6$ MHz, and $V_{trig} = 2.5$ V [26]. Spectrometer 3 ($S3$) was a frequency-agile, rapid scanning (FARS) CRDS [38] instrument with nominal $L = 74$ cm, $\ell = 3.0 \times 10^{-5}$, $\delta \approx 130$ Hz, NEP $= 0.34$ pw Hz$^{-1/2}$ and $B = 300$ kHz, and $V_{trig} = 2$ V [39]. As a result of their design, the spectrometer empty-cavity time constants spanned 1 order of magnitude (from 14.9 $\mu$s for $S2$ to 142 $\mu$s for $S1$), thus providing substantially different working parameters over which to evaluate digitizer biases. The considerable differences in number and identity of optical components and their alignment also aided to randomize baseline effects (e.g., etalons) between spectrometers, and variations in spectral sampling density and spectral window also served to randomize differences between the measurements.

To test for variations in digitizer nonidealities, cavity decays from each spectrometer $S1$–$S3$ were digitized either by the reference digitizer, one of several calibrated digitizers, or both. The reference digitizer (National Instruments PCI-5922) was a highly linear digitizer that has found application in alternating-current (ac) electrical metrology [40–41]. As such, the reference digitizer (hereafter also referred to as $D1$) was used as a transfer standard to compare the performance of other digitizers ($D2$–$D5$), which while common in CRDS have not been adequately characterized for their conversion fidelity. A summary of our independent evaluation of $D1$'s static linearity (dc to 10 kHz) is available in the Supplemental Material [42].

In brief, the calibrated digitizers $D2$–$D5$ were each a direct-current (dc) coupled, full-sized peripheral-component interconnect express digitizer board with sampling rate $F_s = 200$ MS/s, digitization bandwidth $B = 125$ MHz, vertical range $V_{pp} = \pm 10$ V, and vertical resolution $\Delta = 16$ bits. The calibrated digitizers $D2$–$D5$ were evaluated with respect to the reference digitizer $D1$ using SEDS from an arbitrary waveform generator (Agilent M8190A operating at $F_s = 128$ MS/s). The SEDS acted as a proxy for a full dc-ac analysis [40–42] and enabled a direct evaluation of $D2$–$D5$ performance for CRDS. When necessary to reproduce experimental conditions, SEDS were amplified and offset prior to evaluation by the reference digitizer using linear analog electronics including amplifiers, dc voltage sources, and/or a summing amplifier with 1 MHz of electronic bandwidth and total harmonic distortion of $\leq 10^{-4}$ at 1 kHz (Stanford Research Systems Small Instrument Modules). The SEDS time constants measured by the reference digitizer $D1$ ($\tau_{SEDS}$) were used to calibrate the apparent time constants ($\tau_A$) measured by digitizers $D2$–$D5$. The resulting $D2$–$D5$ calibration coefficients $b_1$ and $b_0$ from the fitted equation $\tau_{SEDS} = b_1\tau_A + b_0$ are listed in the Supplemental Material [42], along with the empty-cavity $\tau$ ($\tau_0$) measured for spectrometers $S1$–$S3$. Digitizers were interchanged in some instances, resulting in the following six unique combinations of digitizer and spectrometer: $D1$–$S1$, $D1$–$S3$, $D2$–$S3$, $D3$–$S1$, $D4$–$S2$, and $D5$–$S2$. We therefore report a comparison across six values of $S$ for the $R$ 16$e$ transition within the 30012—00001 band of $^{12}C^{16}O_2$.

The $b_1$ and $b_0$ digitizer calibration coefficients were used to calculate cavity time constants ($\tau$) from the measured $\tau_A$ by the equation $\tau = b_1\tau_A + b_0$, and therefore resulted in absorption spectra of $CO_2$ that were corrected for bias introduced by the digitizers. The empirical procedure outlined above ensured that all values of $\tau$ measured by each unique digitizer-spectrometer combination were linked to the metrology-grade reference digitizer $D1$ with high static linearity [40–42]. Note that the empirical $D2$–$D5$ calibration procedure accounted for all sources of electronic distortion and/or bias from the photoreceiver output to the digitizer input, as well as biases inherent to $D2$–$D5$. For all cases, the $b_1$ and $b_0$ coefficients were determined by replacing the spectrometer photoreceiver output with the SEDS, thus evaluating the entire electronic chain for each respective $S1$–$S3$ instrument preceding $D2$–$D5$. The electronic chain preceding each digitizer was unique for each spectrometer, and, e.g., included various electronic cables and splitters, delay generators, filters, and/or additional digitizers and oscilloscopes which could result in unwanted back reflections, impedance mismatches, thermoelectric voltages from dissimilar connector metals, and various types of ac pickup and interference. When using the reference digitizer $D1$ to measure $S$ ($D1$–$S1$ and $D1$–$S3$), no calibrations were performed,

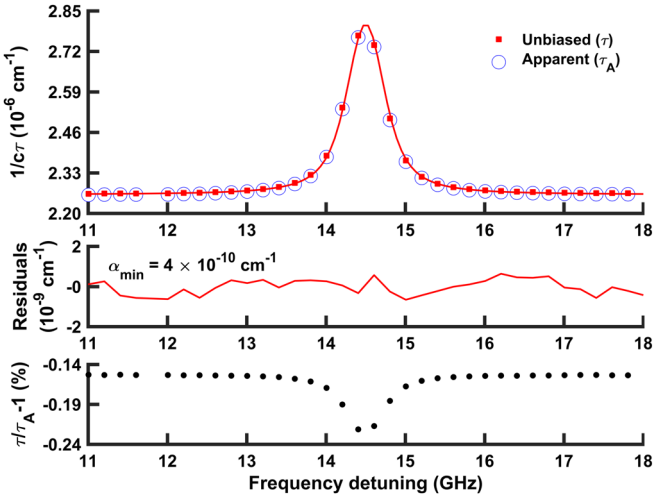


FIG. 2. A portion of representative unbiased (red squares) and apparent (blue circles) spectra of the $R$ 16$e$ $CO_2$ transition with $\tilde{\nu}_0 = 6359.967$ cm$^{-1}$ are shown in the top panel. Fitted spectra spanned a frequency detuning range of 0–28 GHz, the sample pressure was 8.88 kPa, and the sample $CO_2$ mole fraction was $\chi_{CO_2} = (387.98 \pm 0.05)$ $\mu$mol/mol. The apparent spectrum was recorded by the digitizer-spectrometer combination $D4$–$S2$, and $\tau_A$ were corrected to yield $\tau$ using the coefficients in the Supplemental Material [42]. A fitted model of the unbiased absorption coefficient ($\alpha = 1/c\tau$) is also shown as a red line and fitted residuals are plotted as another red line in the middle panel. In the bottom panel, the relative difference $\tau/\tau_A - 1$ (equal to $\alpha_A/\alpha - 1$, where $\alpha_A$ is the apparent absorption coefficient) is plotted as black dots.

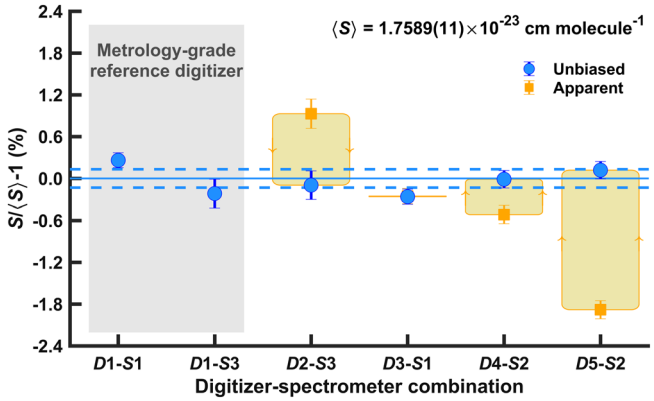


FIG. 3. Unbiased ($S$, blue circles) and apparent ($S_A$, orange squares) values of the $R$ 16$e$ $CO_2$ line intensity at $T = 296$ K (30012—00001 band). Error bars show $\pm 1\sigma$ standard uncertainties. The gray shaded region comprising $D1$–$S1$ and $D1$–$S3$ (far left) highlights values of $S$ measured by the metrology-grade reference digitizer. For values of $S$ with corresponding values of $S_A$, light orange boxes indicate the magnitude of each digitizer correction. The light blue dashed lines bound the standard deviation of the weighted mean value of $S$ (solid blue line).

and all efforts were made to minimize biases associated with the up-stream electrical chain.

Representative unbiased and apparent spectra of the $R$ 16$e$ transition within the 30012—00001 $^{12}C^{16}O_2$ band recorded using the $D4$–$S2$ combination and a sample pressure of 8.88 kPa are plotted in Fig. 2. Shown in blue open circles are the apparent loss-per-unit length [sample absorption coefficient plus base losses equal to $\alpha_A(\nu) = 1/c\tau_A(\nu)$ in units of cm$^{-1}$]. The unbiased values [$\alpha(\nu) = 1/c\tau(\nu)$] are shown as solid red squares, along with the corresponding fitted model (red line). The fitted residuals are also plotted as a red line in the middle panel. In the bottom panel of Fig. 2, the relative difference between the apparent and unbiased absorption coefficients ($\alpha_A/\alpha - 1 = \tau/\tau_A - 1$) is plotted as black dots. To model the experimental line shapes, we used the speed-dependent Nelkin-Ghatak profile, a limiting case of the Hartmann-Tran profile [43]. The spectral model for fitting was completed by including a linear baseline function and, when necessary, sine functions to model undesired optical etalons.

For each digitizer-spectrometer combination, line areas $A = \int \alpha(\nu) d\nu$ were measured at a minimum of four pressures over the range of 8.7–27 kPa (65–200 Torr). Linear fits of $A$ versus absorber number density ($\rho = p/k_B T$) yielded $S$ for the $R$ 16$e$ $CO_2$ transition (corrected to $T = 296$ K using the known $CO_2$ total partition function and lower state energy [29,44]). The individual $S$ values are tabulated in the Supplemental Material [42], along with the apparent values ($S_A$) extracted from linear fits of the apparent line areas $A_A = \int \alpha_A(\nu) d\nu$ versus $\rho$, the relative changes in $S_A$ following calibration, and the individual relative standard uncertainties $u_{i,r}(S)$. Even at the highest pressure of 27 kPa, we observe no evidence of significant collisional effects beyond the impact approximation like those investigated for polar molecules like HF and HCl in high-pressure ($p > 200$ kPa) buffer gases of Xe and Ar, respectively [45,46]. No systematic deviations in the residuals of the linear fits of $A$ versus $\rho$ were observed. Because the buffer-gas effects (e.g., dimerization) decrease rapidly with increasing rotational quantum number $J$, we anticipate little effect on the retrieved values of $S$ at $T = 296$ K for the $J = 16$ transition of $CO_2$.

Plotted, respectively, in Fig. 3 are the unbiased $S$ (blue circles) and apparent $S_A$ (orange squares) values for each digitizer-spectrometer combination relative to the weighted mean value of $S = (1.7589 \pm 0.0011) \times 10^{-23}$ cm/molecule, where the weighting factors for calculating $S$ were $w_i = u_i^{-2}$. Although the $u_i(S)$ values comprised both type-$A$ and type-$B$ uncertainties [42], we assumed that the individual type-$B$ (systematic) uncertainties attributed to each unique digitizer-spectrometer combination were uncorrelated with respect to the other combinations. For example, the individual type-$B$ uncertainties related to sample temperature ($T$) were considered uncorrelated because each spectrometer utilized a different temperature

probe and mounting configuration. Assuming $u_i(S)$ were uncorrelated, we estimated the type-$A$ uncertainty in our final value of $S$ to equal the standard error of the weighted mean of all six digitizer-spectrometer combinations [$u_{r,A}(S) = 0.059\%$]. In addition to $u_{r,A}(S)$, the combined relative uncertainty budget for $S$ also included two type-$B$ uncertainties common to all digitizer-spectrometer combinations: uncertainty in the sample mole fraction of 0.013% and uncertainty in our evaluation of the static linearity of the reference digitizer $D1$ of 0.002% [42]. A quadrature sum of uncertainties yielded the reported relative standard uncertainty of $u_r(S) = 0.06\%$, dominated by $u_{r,A}(S)$. The reported value of $u_r(S) = 0.06\%$ is a more than sixfold reduction in uncertainty as compared to that calculated from values of $S_A$ (0.4%), and a more than 25-fold improvement as compared to the literature [$u_{\mathrm{lit}}(S) \approx 2\%$] [29].

Figure 3 shows that we identified and corrected (orange boxes) a previously uncharacterized source of significant systematic (type-$B$) uncertainty in high-precision CRDS: digitization nonidealities. Using an empirical calibration procedure and a metrology-grade reference digitizer, the newly considered digitizer bias was largely removed, and independent measurements of a molecular line intensity converged to within the measurement precision. By comparison across multiple unique CRDS instruments, we randomized any remaining type-$B$ uncertainties inherent to our spectroscopic approach or individual instrumentation and significantly reduced the relative combined uncertainty to below the $10^{-3}$ level. In the future, additional independent measurements will therefore provide further statistical reduction in uncertainty. Furthermore, comparisons between various types of cavity-enhanced spectroscopies [47] would provide valuable independent checks of our CRDS-based measurement approach.

The digitizer bias correction procedure presented here, with traceability to an electrical metrology-grade reference digitizer [40,41], is applicable to stand-alone instruments and could be used to generally confirm or improve the accuracy of measured cavity ring-down spectroscopy decay times. The realization of accurate and precise measurements of line intensities below the $10^{-3}$ level opens the possibility of pushing against other measurement boundaries related to sample conditions (e.g., temperature, pressure, absorber mole fraction). Ultimately, referencing digitizer static linearity at both $V_{\mathrm{dc}}$ and $V_{\mathrm{ac}}$ to traceable electrical metrology tools linked to the new international system of units [48,49], or quantum SI, could enable accuracy and SI traceability for direct absorption spectroscopy below the $10^{-4}$ level.

We acknowledge Jason Underwood and Stefan Cular (National Institute of Standards and Technology, NIST) for discussions regarding electrical metrology and digitizer characterization and Christopher W. Meyer (NIST) for a multimeter instrument loan. We also acknowledge funding from the NIST Greenhouse Gas and Climate Science Program and from NASA Spectroscopy in Support of the OCO Missions. Certain commercial equipment is identified in this paper in order to specify the experimental procedure adequately. Such identification is not intended to imply recommendation or endorsement by the National Institute of Standards and Technology, nor is it intended to imply that the equipment identified is necessarily the best available for the purpose.

*Corresponding author.
adam.fleisher@nist.gov
†Corresponding author.
joseph.hodges@nist.gov

[1] J. Li, M. Holzmann, I. Duchemin, X. Blase, and V. Olevano, Helium Atom Excitations by the *GW* and Bethe-Salpeter Many-Body Formalism, Phys. Rev. Lett. **118**, 163001 (2017).
[2] J. Bagdonaite, W. Ubachs, M. T. Murphy, and J. B. Whitmore, Constraint on a Varying Proton-Electron Mass Ratio 1.5 Billion Years After the Big Bang, Phys. Rev. Lett. **114**, 071301 (2015).
[3] W. Ubachs, J. C. J. Koelemeij, K. S. E. Eikema, and E. J. Salumbides, Physics beyond the standard model from hydrogen spectroscopy, J. Mol. Spectrosc. **320**, 1 (2016).
[4] W. Ubachs, Search for varying constants of nature from astronomical observations of molecules, Space Sci. Rev. **214**, 3 (2018).
[5] P. R. Mahaffy, C. R. Webster, S. K. Atreya, H. Franz, M. Wong, P. G. Conrad, D. Harpold, J. J. Jones, and L. A. Leshin (MSL Science Team), Abundance and isotopic composition of gases in the Martian atmosphere from the Curiosity Rover, Science **341**, 263 (2013).
[6] K. Lind, J. Melendez, M. Asplund, R. Collet, and Z. Magic, The lithium isotopic ratio in very metal-poor stars, Astron. Astrophys. **554**, A96 (2013).
[7] O. L. Polyansky, K. Bielska, M. Ghysels, L. Lodi, N. F. Zobov, J. T. Hodges, and J. Tennyson, High-Accuracy $CO_2$ Line Intensities Determined from Theory and Experiment, Phys. Rev. Lett. **114**, 243001 (2015).
[8] T. Karman, M. A. J. Koenis, A. Banerjee, D. H. Parker, I. E. Gordon, A. van der Avoird, W. J. van der Zande, and G. C. Groenenboom, $O_2$-$O_2$ and $O_2$-$N_2$ collision-induced absorption mechanisms unraveled, Nat. Chem. **10**, 549 (2018).
[9] J. Tennyson, S. N. Yurchenko, A. F. Al-Refaie, E. J. Barton, K. L. Chubb, P. A. Coles, S. Diamantopoulou, M. N. Gorman, C. Hill, A. Z. Lam *et al.*, The ExoMol database: Molecular line lists for exoplanet and other hot atmospheres, J. Mol. Spectrosc. **327**, 73 (2016).
[10] A. Kuze, H. Suto, M. Nakajima, and T. Hamazaki, Thermal and near infrared sensor for carbon observation Fourier-transform spectrometer on the greenhouse gases observing satellite for greenhouse gases monitoring, Appl. Opt. **48**, 6716 (2009).
[11] D. Crisp, R. M. Atlas, F.-M. Breon, L. R. Brown, J. P. Burrows, P. Ciais, B. J. Conner, S. C. Doney, I. Y. Fung, D. J. Jacob *et al.*, The orbiting carbon observatory (OCO) mission, Adv. Space Res. **34**, 700 (2004).

[12] C. E. Miller, L. R. Brown, R. A. Toth, D. C. Benner, and V. M. Devi, Spectroscopic challenges for high accuracy retrievals of atmospheric $CO_2$ and the orbiting carbon observatory (OCO) experiment, C.R. Phys. **6**, 876 (2005).

[13] F. M. Schwandner, M. R. Gunson, C. E. Miller, S. A. Carn, A. Eldering, T. Krings, K. R. Verhulst, D. S. Schimel, H. M. Nguyen, D. Crisp *et al.*, Spaceborne detection of localized carbon dioxide sources, Science **358**, eaam5782 (2017).

[14] P. Bergamaschi, C. Frankenberg, J. F. Meirink, M. Krol, M. G. Villani, S. Houweling, F. Dentener, E. J. Dlugokencky, J. B. Miller, L. V. Gatti, *et al.*, Inverse modeling of global and regional $CH_4$ emissions using SCIAMACHY satellite retrievals, J. Geophys. Res. Atmos. **114**, D22301 (2009).

[15] R. Parker, H. Boesch, A. Cogan, A. Fraser, L. Feng, P. I. Palmer, J. Messerschmidt, N. Deutscher, D. W. T. Griffith, J. Notholt *et al.*, Methane observations from the greenhouse gases observing SATellite: Comparison to ground-based TCCON data and model calculations, Geophys. Res. Lett. **38**, L15807 (2011).

[16] C. Stephan, M. Alpers, B. Millet, G. Ehret, P. Flamant, and C. Deniel, MERLIN: Aspace-based methane monitor, in *Lidar Remote Sensing for Environmental Monitoring XII*, Proceedings Volume 8159 of the SPIE (SPIE-International Society for Optical Engineering, Bellingham, WA, 2011), p. 815908, https://doi.org/10.1117/12.896589.

[17] H. Riris, K. Numata, S. Li, S. Wu, A. Ramanathan, M. Dawsey, J. Mao, R. Kawa, and J. B. Abshire, Airborne measurements of atmospheric methane column abundance using a pulsed integrated-path differential absorption lidar, Appl. Opt. **51**, 8296 (2012).

[18] J. Tollefson, Big prize for methane probe, Nature (London) **556**, 283 (2018).

[19] S. Coburn, C. B. Alden, R. Wright, K. Cossel, E. Baumann, G.-W. Truong, F. Giorgetta, C. Sweeney, N. R. Newbury, K. Prasad *et al.*, Regional trace-gas source attribution using a field-deployable dual frequency comb spectrometer, Optica **5**, 320 (2018).

[20] T. Delahaye, S. E. Maxwell, Z. D. Reed, H. Lin, J. T. Hodges, K. Sung, V. M. Devi, T. Warneke, P. Spietz, and H. Tran, Precision methane absorption measurements in the 1.64 μm spectral region for the MERLIN mission, J. Geophys. Res. Atmos. **121**, 7360 (2016).

[21] T. Delahaye, M. Ghysels, J. T. Hodges, K. Sung, R. Armante, and H. Tran, Measurement and modeling of air-broadened methane absorption in the MERLIN spectral region at low temperatures, J. Geophys. Res. Atmos. **124**, 3556 (2019).

[22] E. M. Waxman, K. C. Cossel, G.-W. Truong, F. R. Giorgetta, W. C. Swann, S. Coburn, R. J. Wright, G. B. Rieker, I. Coddington, and N. R. Newbury, Intercomparison of open-path trace gas measurements with two dual-frequency-comb spectrometers, Atmos. Meas. Tech. **10**, 3295 (2017).

[23] P. F. Bernath, The atmospheric chemistry experiment (ACE), J. Quant. Spectrosc. Radiat. Transfer **186**, 3 (2017).

[24] G. Ycas, F. R. Giorgetta, E. Baumann, I. Coddington, D. Herman, S. A. Diddams, and N. R. Newbury, High-coherence mid-infrared dual-comb spectroscopy, Nat. Photonics **12**, 202 (2018).

[25] G. Ycas, F. R. Giorgetta, K. C. Cossel, E. M. Waxman, E. Baumann, N. R. Newbury, and I. Coddington, Mid-infrared dual-comb spectroscopy of volatile organic compounds across long open-air paths, Optica **6**, 165 (2019).

[26] H. Yi, Q. Liu, A. J. Fleisher, and J. T. Hodges, High-accuracy $^{12}C^{16}O_2$ line intensities in the 2 $\mu$m wavelength region measured by frequency-stabilized cavity ring-down spectroscopy, J. Quant. Spectrosc. Radiat. Transfer **206**, 367 (2018).

[27] P. Guay, J. Genest, and A. J. Fleisher, Precision spectroscopy of $H^{13}CN$ using a free-running, all-fiber dual electro-optic frequency comb system, Opt. Lett. **43**, 1407 (2018).

[28] V. Yu. Makhnev, A. A. Kyuberis, O. L. Polyansky, I. I. Mizus, J. Tennyson, and N. F. Zobov, A new spectroscopically-determined potential energy surface and *ab initio* dipole moment surface for high accuracy HCN intensity calculations, J. Mol. Spectrosc. **353**, 40 (2018).

[29] I. E. Gordon, L. S. Rothman, C. Hill, R. V. Kochanov, Y. Tan, P. F. Bernath, M. Birk, V. Boudon, A. Campargue, K. V. Chance, *et al.*, The HITRAN2016 molecular spectroscopic database, J. Quant. Spectrosc. Radiat. Transfer **203**, 3 (2017).

[30] F. Oyafuso, V. H. Payne, B. J. Drouin, V. M. Devi, D. C. Benner, K. Sung, S. Yu, I. E. Gordon, R. Kochanov, Y. Tan *et al.*, High accuracy absorption coefficients for the orbiting carbon observatory-2 (OCO-2) mission: Validation of updated carbon dioxide cross-sections using atmospheric spectra, J. Quant. Spectrosc. Radiat. Transfer **203**, 213 (2017).

[31] S. R. Kawa, J. Mao, J. B. Abshire, G. J. Collatz, X. Sun, and C. J. Weaver, Simulation studies for a space-based $CO_2$ lidar mission, Tellus B **62**, 759 (2010).

[32] G. Giusfredi, S. Bartalini, S. Borri, P. Cancio, I. Galli, D. Mazzotti, and P. De Natale, Saturated-Absorption Cavity Ring-Down Spectroscopy, Phys. Rev. Lett. **104**, 110801 (2010).

[33] S. Wójtewicz, D. Lisak, A. Cygan, J. Domysławska, R. S. Trawiński, and R. Ciuryło Line-shape study of self-broadened $O_2$ transitions measured by Pound-Drever-Hall-locked frequency-stabilized cavity ring-down spectroscopy, Phys. Rev. A **84**, 032511 (2011).

[34] G. C. Rhoderick, M. E. Kelley, W. R. Miller, G. Brailsford, and A. Possolo, Development of a southern oceanic air standard reference material, Anal. Bioanal. Chem. **408**, 1159 (2016).

[35] Assuming $\delta^{13}C = -8.3‰$ and $\delta^{18}O = 1.0‰$ (Vienna Pee Dee Belemnite $CO_2$ scale) for the SRM gas sample reported in Ref. [34], we estimated the mole fraction of $^{12}C^{16}O_2$ to be $\chi_{626} = 0.984\,124\,47\chi_{CO_2}$. Note that the accurate value of $S$ reported herein was scaled to $\chi_{626} = 0.984\,204$ adopted by HITRAN2016 [29]; a relative adjustment of only 0.008%.

[36] J. T. Hodges, H. P. Layer, W. W. Miller, and G. E. Scace, Frequency-stabilized single-mode cavity ring-down apparatus for high-resolution absorption spectroscopy, Rev. Sci. Instrum. **75**, 849 (2004).

[37] H. Lin, Z. D. Reed, V. T. Sironneau, and J. T. Hodges, Cavity ring-down spectrometer for high-fidelity molecular absorption measurements, J. Quant. Spectrosc. Radiat. Transfer **161**, 11 (2015).

[38] G.-W. Truong, K. O. Douglass, S. E. Maxwell, R. D. van Zee, D. F. Plusquellic, J. T. Hodges, and D. A. Long, Frequency-agile, rapid scanning spectroscopy, Nat. Photonics **7**, 532 (2013).

[39] D. A. Long, S. Wójtewicz, C. E. Miller, and J. T. Hodges, Frequency-agile, rapid scanning cavity ring-down spectroscopy (FARS-CRDS) measurements of the $(30012) \leftarrow (00001)$) near-infrared carbon dioxide band, J. Quant. Spectrosc. Radiat. Transfer **161**, 35 (2015).

[40] F. Overney, A. Rüfenacht, J.-P. Braun, B. Jeanneret, and P. S. Wright, Characterization of metrological grade analog-to-digital converters using a programmable Josephson voltage standard, IEEE Trans. Instrum. Meas. **60**, 2172 (2011).

[41] G. Rietveld, D. Zhao, C. Kramer, E. Houtzager, O. Kristensen, C. de Leffe, and T. Lippert, Characterization of a wideband digitizer for power measurements up to 1 MHz, IEEE Trans. Instrum. Meas. **60**, 2195 (2011).

[42] See Supplemental Material at http://link.aps.org/supplemental/10.1103/PhysRevLett.123.043001 for a summary of the reference digitizer $D1$ comparisons with the high-precision multimeter, as well as the individual digitizer-spectrometer data including calibration coefficients ($b_1$, $b_0$), empty-cavity time constants ($\tau_0$), measured apparent ($S_A$) and unbiased ($S$) line intensities, the relative changes in line intensities, relative combined uncertainties ($u_r$), and a representative uncertainty budget.

[43] J. Tennyson, P. F. Bernath, A. Campargue, A. G. Császár, L. Daumont, R. R. Gamache, J. T. Hodges, D. Lisak, O. V. Naumenko, L. S. Rothman, *et al.*, Recommended isolated-line profile for representing high-resolution spectroscopic transitions (IUPAC Technical Report, Pure Appl. Chem. **86**, 1931 (2014).

[44] R. R. Gamache, C. Roller, E. Lopes, I. E. Gordon, L. S. Rothman, O. L. Polyansky, N. F. Zobov, A. A. Kyuberis, J. Tennyson, S. N. Yurchenko, *et al.*, Total internal partition sums for 166 isotopologues of 51 molecules important in planetary atmospheres: Application to HITRAN2016 and beyond, J. Quant. Spectrosc. Radiat. Transfer **203**, 70 (2017).

[45] A. P. Kouzov, K. G. Tokhadze, and S. S. Utkina, Buffer-gas effects on the rotovibrational line intensity distribution: Analysis of possible mechanisms, Eur. Phys. J. D **12**, 153 (2000).

[46] C. Boulet, P.-M. Flaud, and J.-M. Hartmann, Infrared line collisional parameters of HCl in argon, beyond the impact approximation: Measurements and classical path calculations, J. Chem. Phys. **120**, 11053 (2004).

[47] A. Cygan, S. Wójtewicz, G. Kowzan, M. Zaborowski, P. Wcisło, J. Nawrocki, P. Krehlik, Ł. Śliwczyński, M. Lipiński, P. Masłowski, *et al.*, Absolute molecular transition frequencies measured by three cavity-enhanced spectroscopy techniques, J. Chem. Phys. **144**, 214202 (2016).

[48] C. J. Burroughs, Jr., P. D. Dresselhaus, A. Rüfenacht, D. Olaya, M. M. Elsbury, Y.-H. Tang, and S. P. Benz, NIST 10 V programmable Josephson voltage standard system, IEEE Trans. Instrum. Meas. **60**, 2482 (2011).

[49] N. E. Flowers-Jacobs, A. E. Fox, P. D. Dresselhaus, R. E. Schwall, and S. P. Benz, Two-volt Josephson arbitrary waveform synthesizer using Wilkinson dividers, IEEE Trans. Appl. Supercond. **26**, 1400207 (2016).